Investigation of the s-shape caused by the hole selective layer in bulk heterojunction solar cells

Lothar Sims[a,b,*], Ulrich Hörmann[a], Robert Hanfland[a], Roderick C.I. MacKenzie[c], F. René Kogler[d], Roland Steim[e], Wolfgang Brütting[a], Pavel Schilinsky[b]

[a]*University of Augsburg, Institute of Physics, Universitätsstr. 1, 86135 Augsburg, Germany*

[b]*Belectric OPV GmbH, Landgrabenstr. 94, 90443 Nürnberg, Germany*

[c]*Faculty of Engineering, University of Nottingham, Nottingham, NG7 2RD UK*

[d]*Konarka Technologies GmbH, Landgrabenstr. 94, 90443 Nürnberg, Germany*

[e]*Laboratory for Functional Polymers, Empa Swiss Federal Laboratories for Materials Science and Technology, Überlandstr. 129, 8600 Dübendorf, Switzerland*

A common failure mechanism of organic solar cells is the development of an s-shaped current voltage curve. Herein, we investigated the origin of this degradation mechanism by replacing the commonly used hole selective layer poly(3,4-ethylenedioxythiophene) poly(styrenesulfonate) (PEDOT:PSS) with a co-evaporated layer of N,N'-bis(3-methylphenyl)-N,N'-bis(phenyl)-benzidine (TPD) and Dipyrazino[2,3-f:2',3'-h]quinoxaline-2,3,6,7,10,11-hexacarbonitrile (HATCN). By varying the ratio of TPD to HATCN we are able to tune both the mobility and work function of the hole selective layer. Using a combination of field effect mobility measurements, Kelvin-Probe work function measurements, and

* Corresponding author.
E-mail address: lothar.sims@physik.uni-augsburg.de (L.Sims)

numerical modeling we demonstrate that a degraded mobility of the hole selective layer leads to a buildup of charge within the device and reduction of fill factor.

1. Introduction

Over the last 12 years intense research has increased the efficiency of organic solar cells (OSC) from 2 % in 2002 [1],[2],[3],[4] to over 12 % [5],[6] today. For OSCs to become a commercial reality, cost per Watt of energy produced must be reduced [7], device area must increase from lab scales (< 1 cm^2) to industrial scales (> 30 cm^2) [8] and low throughput spin coating fabrication techniques must be replaced with high throughput (> 40 m/min) roll-to-roll production methods such as gravure printing [9]. Another important aspect which has received less attention to date is long term device stability and the physical mechanisms responsible for the reduction of device performance over time. A common degradation mechanism in organic solar cells is the development of an s-shaped current voltage (JV) curve. In this failure mechanism the maximum power point in the 4^{th} quadrant of the JV-curve moves towards the origin over time. This leads to a reduction of the fill factor (FF), often to below 25 %. Various mechanisms for the development of an s-shaped JV-curve have been proposed in literature.

Wagenpfahl et al. found that a reduced surface recombination velocity at the hole selective layer (HSL)/active layer interface hinders efficient hole extraction [10]. Accumulated holes then produce unfavorable band bending which hinders carrier extraction and lead to an s-shape. While Castro et al. investigated interpenetrating bilayer OSCs [11], they suggested that isolated aluminum nanoclusters are formed in the active layer close to the aluminum/active layer interface upon evaporation. These nanoclusters then act as trap states modifying the electric potential within the device. Wagner et al. showed that trap states in the active layer cannot only be induced by top electrode diffusion but also caused by impurities in the active

material itself and confirmed that injection barriers may cause s-shapes in the case of planar heterojunctions [12]. Further, Tress et al. suggested that in bilayer devices, when the electron and hole mobility differ by more than two orders of magnitude, s-shapes will be observed [13]. Finally, they found that in the case of both, bilayer and blend structures, extraction barriers, i.e. a mismatch of the HOMOs of donor and HSL can be responsible for the s-shape [14].

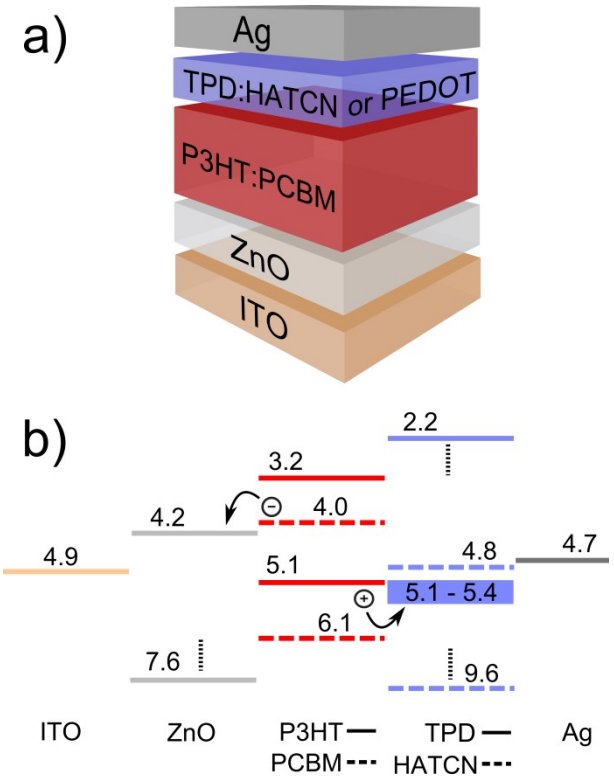

Figure 1 - a) Layer sequence of the investigated OSCs. b) Energy levels of ITO and Ag were obtained by KP-measurements, the other values are from literature [15],[16],[17],[18],[19]. Vertical dashed lines indicate discontinuities.

In this work, we investigate the physical relationship between degradation of the electrical properties of the hole selective layer and the development of an s-shaped JV-curve in an inverted organic solar cell. Reasons for degradation can be, amongst others, ingress of oxygen

or water [20],[21]. To understand how this degradation process influences device performance, we replace the commonly used poly(3,4-ethylenedioxythiophene) poly(styrenesulfonate) (PEDOT:PSS) HSL, with a model material system comprising of co-evaperated N,N'-bis(3-methylphenyl)-N,N'-bis(phenyl)-benzidine (TPD) and Dipyrazino[2,3-f:2',3'-h]quinoxaline-2,3,6,7,10,11-hexacarbonitrile (HATCN). By tuning the ratio of TPD to HATCN we are able to control both mobility and work function of the HSL. Compared to the work by Tress et al. mentioned above [13], we show that s-shapes due to improper mobility also happen in bulk heterojunction devices. Moreover, by changing the TPD:HATCN ratio we are able to vary the mobility quasi continuously which was not possible in the work by Tress et al.. For the bulk heterojunction we use the standard poly(3-hexylthiophene-2,5-diyl):[6,6]-phenyl C_{61} butyric acid methyl ester (P3HT:PCBM) materials. A diagram of the inverted device structure and the band structure can be seen in Figure 1.

2. Experimental

Inverted OSCs were prepared on flexible PET substrates with ITO as the transparent electrode. First an 80 nm thick layer of ZnO nanoparticles was deposited from solution onto the ITO in air with doctor blading [22]. The ZnO layer was then annealed at 140 °C for 5 minutes in ambient air. Subsequently, 300 nm of P3HT mixed with [6,6]-phenyl C_{61} butyric acid methyl ester (PCBM) in the ratio 1:0.8 by weight were doctor bladed onto the ZnO layer. The cells were transferred into a nitrogen filled glove box and annealed at 140 °C for 5 minutes, to remove any free oxygen trapped in the material. The HSL was then deposited by evaporation (14 nm) at $1x10^{-6}$ mbar. The following HSLs were used: pure TPD, a mixture of TPD:HATCN, and pure HATCN. The ratio of HATCN was varied between 1 and 10 % relative to the TPD amount with an estimated absolute error of about 0.5%. The cells were finished with a 150 nm thick layer of evaporated silver as top electrode.

Reference cells were also fabricated by doctor blading the more standard Poly(3,4-ethylenedioxythiophene)-poly(styrenesulfonate) (PEDOT:PSS, Clevios PH) as the HSL. JV-curves were measured under simulated AM1.5G illumination with an intensity of 100 mW/cm^2. For mobility measurements organic field effect transistors (OFETs) were prepared using a p-doped silicon wafer covered with a 230 nm thick SiO_2 layer and interdigitated gold finger electrodes with different channel lengths of 5, 10, 15 and 20 µm. All devices fabricated had a channel width of 1.2 cm and an active layer thickness of 14 nm. Work functions were determined by Kelvin-Probe (KP) measurements using ITO covered PET as substrate and highly oriented graphite with a work function of 4.65 eV as reference. The OFETs as well as the devices for KP-measurements were evaporated simultaneously with the OSCs. After preparation the samples were not removed from the glove box until all electrical measurements were completed.

3. Results and discussion

JV-curves of solar cells with hole selective layers comprising of pure TPD and mixtures of TPD:HATCN under AM 1.5G illumination are shown in Figure 2a. It can be seen that for pure TPD (black squares) the s-shape is most pronounced, with increasing HATCN content the s-shape reduces then vanishes (blue triangles). It can also be seen that the open circuit voltage (V_{oc}) and FF are a function of the TPD:HATCN ratio. Plotted in Figure 2b are the JV-curves of pure pristine TPD (black squares) and aged TPD (black open squares). Upon aging of the TPD layer the s-shape reduces. Also plotted in Figure 2b are the JV-curves for pure HATCN (turquoise diamonds), and for a device with the more commonly used PEDOT:PSS (grey dots) HSL. Interestingly, both pure HATCN and PEDOT:PSS have identical JV-curves, suggesting carrier extraction is equally efficient for both materials.

HATCN was used in combination with C60 electron selective layers before by Falkenberg et al. [17]. The reason why HATCN works as HSL can be explained as follows. The transistor

measurements show that electrons in the HATCN LUMO are present (Figure S1) which is crucial for hole extraction when pure HATCN is applied as HSL in solar cells. Electrons from the Ag electrode are transferred to the HATCN LUMO and recombine with holes coming from the P3HT layer. This is essentially equivalent to holes being extracted and similar to the working mechanism of MoO_3 whose conduction and valence band are in a similar range as the LUMO and HOMO of HATCN [23]. Consequently, in the case of hole injection under forward bias electrons are extracted from the P3HT HOMO via the HATCN LUMO. Thus, the electron mobility of HATCN has to be regarded as relevant mobility of the "hole selective" layer, if pure HATCN is used.

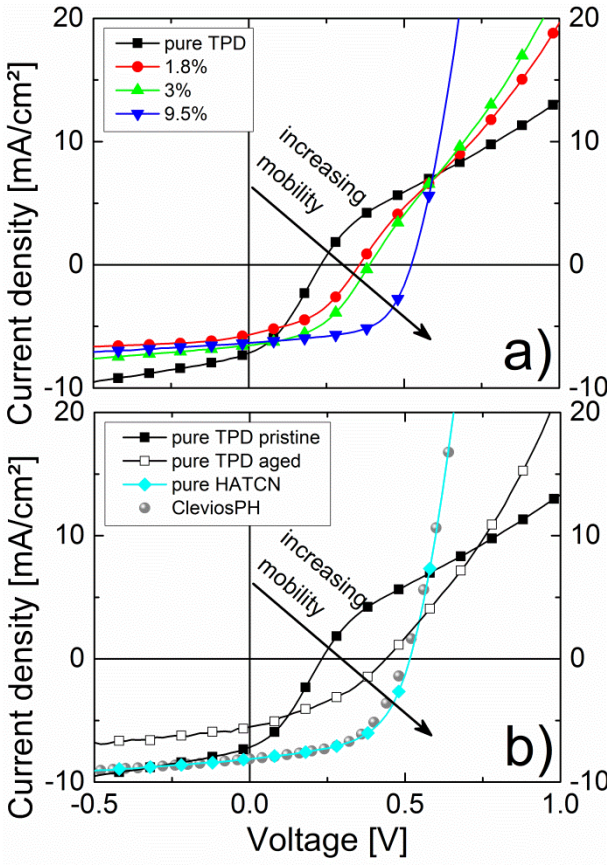

Figure 2 a) JV-curves of samples with pristine pure TPD and TPD:HATCN (1.8, 3.0 and 9.5 %). It can be seen that as HATCN concentration increases the s-shape in the JV-curve reduces. b) The JV-curves for a pure pristine and aged TPD device. Also plotted in the same graph for comparison is a PEDOT:PSS device and a pure HATCN device.

To better understand the reason why increasing the ratio of HATCN in the HSL reduces the s-shape, we investigated the work functions and electrical transport properties for all HSLs used. Figure 3 summarizes the work functions of the different HSLs obtained by KP-measurements. As the ratio of HATCN to TPD is increased we observe an increase in work function which could be interpreted as p-doping. It is possible that a change in the distribution of charge throughout the device, could lead to a change in the built-in voltage and conductivity, which could also alter the JV-curve. The mobility measurements of the different HSL layers in Figure 4 show that with increasing HATCN ratio in TPD also the mobility starts to increase. For a device with 1.8 % HATCN a mobility of 4.1×10^{-7} cm^2/Vs was measured. As the HATCN concentration is further increased to 3 % and 9.5 %, the mobility increases to 4.4×10^{-6} cm^2/Vs and 1×10^{-5} cm^2/Vs, respectively. The mobility of pure TPD directly after deposition is too small for measurement with the OFET method, we were only able to measure down to about $2 \times 10^{-7} cm^2/Vs$ [24]. However, the possibility of p-doping and the increased mobility does not exclude energetic barriers as reason for the s-shape [12], [14].

In the case of pure TPD as HSL the low glass transition temperature of TPD helps to clarify the reason. Upon storage of the pure TPD film in a nitrogen filled glove box at room temperature for 500 h a visual change from a transparent to a matte appearance was observed. When the mobility of the device was re-measured a value of 2.8×10^{-5} cm^2/Vs was obtained. In contrast, for films containing HATCN no visible change took place, neither was a change of mobility measured. This can be explained by TPD having a low glass transition temperature of around 60 °C [25]. Upon aging of the pure TPD film, it changes from an amorphous to a more ordered crystalline film. In case of the TPD:HATCN mixtures a higher thermal stability of TPD in combination with HATCN hinders crystallization of TPD and thus a major change in occurrence and mobility with time [26].

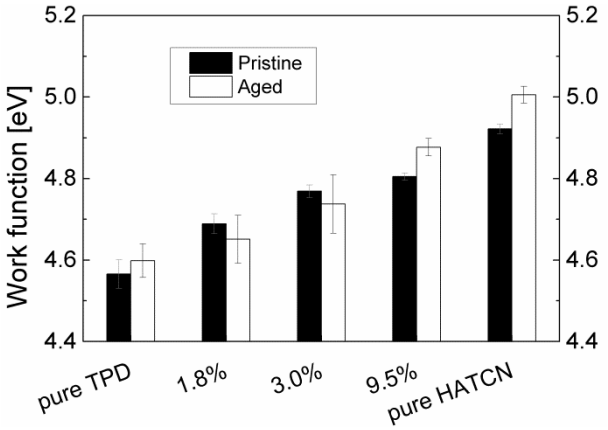

Figure 3 - Work function of pure TPD, TPD:HATCN (1.8, 3.0 and 9.5 %) and pure HATCN on ITO substrates. Black: pristine samples; Open: after 500 h in a nitrogen filled glove box at room temperature.

In contrast, the work function of the pure TPD layer does not change due to crystallization as mobility does. Thus, in the present case we can confirm that the reduction in HSL mobility is the primary cause of the s-shaped JV-curve of the cell with pure TPD by examining Figure 2b, where the JV-curves for a pure pristine and pure aged TPD layer are plotted. As described above when pure TPD is aged (stored in a nitrogen filled glove box), the work function does not change, but the mobility dramatically increases. Upon aging we also see the removal of the s-shape form the JV-curve (Figure 2b). This suggests that it is the mobility which is causing the s-shaped JV-curve in the case of pure TPD as HSL.

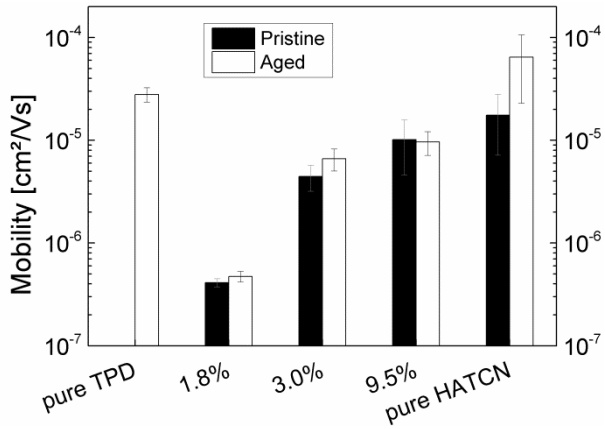

Figure 4 - Mobility of pure TPD, TPD:HATCN (1.8, 3.0 and 9.5 %) and pure HATCN. Black: pristine samples; Open: after 500 h in a nitrogen filled glove box at room temperature. The values are average values of the mobility calculated from the output and transfer characteristic of OFETs. The mobility of pure TPD directly after deposition is too small for measurement with the OFET method, we were only able to measure down to about $2x10^{-7}cm^2/Vs$, thus we only give the value after 500 h storage.

4. Simulation

In order to better understand why an HSL with a decreased mobility will lead to s-shaped JV-curves, we use a steady state Shockley-Read-Hall based drift diffusion model to reproduce the experimental data. The model uses an effective medium approximation [27] whereby only the LUMO of the PCBM and the HOMO of the P3HT are considered in electrical transport. To describe the potential distribution within the device we solve Poisson's equation,

$$\frac{d}{dx}\varepsilon_0\varepsilon_r\frac{d\phi}{dx}=q(n-p) \qquad (1)$$

between the ZnO contact, and the Ag top contact, where ϕ is the electrostatic potential, q is the charge of an electron, n and p are the density of electrons and holes respectively. To describe the transport of electrons and holes within the device we solve the bi-polar drift diffusion equations,

$$J_n = q\,\mu_e n_f \frac{\partial E_{LUMO}}{\partial x} + q\,D_n \frac{\partial n_f}{\partial x}, \quad (2)$$

$$J_p = q\,\mu_h p_f \frac{\partial E_{HOMO}}{\partial x} + q\,D_p \frac{\partial p_f}{\partial x}, \quad (3)$$

where $J_{n/p}$ are the electron/hole current fluxes, $\mu_{e/h}$ are the mobilities, and $E_{LUMO/HOMO}$ are the energy levels of the mobility edges. To describe carrier trapping and recombination the Shockley-Read-Hall recombination model, an exponential distribution of carrier trap states is used. The optical field profile is calculated within the device using a transfer matrix method. The device model has previously been described in more detail elsewhere [28],[29],[30].

Model parameters close to those previously published for the P3HT:PCBM material system were chosen as the starting point for the simulations, these parameters were adjusted until the simulated JV-curve matched that of the device with the highest HATCN concentration (9.5%). Furthermore, in order to simplify the interpretation of the results, symmetric material parameters were chosen (electron values = hole values).

Table I – Mobility as measured and as used for the HSL in the simulated *JV*-curves shown in Figure 5 [31].

Sample	μ [cm²/Vs] (measurement)	μ [cm²/Vs] (simulation)
pure TPD	$1.0\text{x}10^{-7}$ [32]	$1\text{x}10^{-7}$
1.8 % HATCN	$4.1\text{x}10^{-7}$	$4\text{x}10^{-7}$
3.0 % HATCN	$4.4\text{x}10^{-6}$	$1\text{x}10^{-6}$
9.5 % HATCN	$1.0\text{x}10^{-5}$	$1\text{x}10^{-5}$

The first 14 nm of the device next to the hole extracting contact were assigned as the HSL. This layer initially contained the same device parameters as were used within the P3HT:PCBM layer. The hole mobility within this layer was varied to see if s-shaped JV-curves could be generated [31]. The blue line with triangles in Figure 5 shows the simulated JV-curve for a device with a HSL of mobility of $1x10^{-5}$ cm^2/Vs corresponding to a 9.5% HATCN content, plotted against the experimental curve obtained with 9.5% HATCN (grey dots). Also plotted in the same figure are three curves with reduced HSL mobility corresponding to the measured mobility for HATCN concentrations of 0.0%, 1.8% and 3.0%. It can be seen that as the HSL mobility reduces, the JV-curve starts to form an s-shape and the FF reduces. For very low mobilities V_{oc} also starts to reduce a little, however, the major drop in V_{oc} observed experimentally is most likely caused by a change of the work function with different HATCN content, as can be concluded at least qualitatively from Figure 3. For the sake of simplicity this additional parameter has not been included in the simulation.

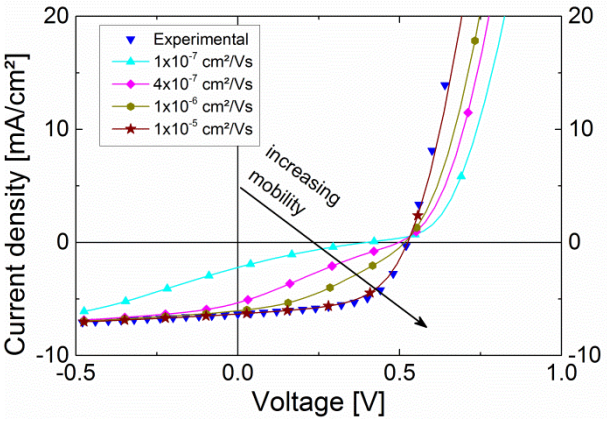

Figure 5 - Simulated *JV*-curves. Pure TPD has the lowest and 9.5 % the highest mobility (see Table I).

Figure 6 plots the average carrier density within the device as a function of hole selective layer mobility. It can be seen that as HSL mobility is increased from $1x10^{-7}$ to $1x10^{-5}$ cm^2/Vs the density of carriers within the device reduces by around 40%. This is because an HSL with a low mobility prevents holes from leaving the device resulting in a buildup of photo generated carriers. By increasing the mobility of the HSL, we enable photo generated carriers to leave the device easily. Also plotted on the same graph is carrier life time as a function of HSL mobility. It can be seen that as HSL mobility increases, carrier lifetime also increases. This is because the charge carrier recombination rate is a function of carrier density ($R = knp$, with k as recombination constant), thus as carrier density in the device increases so does the recombination rate. We can therefore say that by having an HSL with a low mobility, carriers are prevented from leaving the device which in turn increases the recombination rate and thus reduces device efficiency. This reduction in efficiency is the reason for the s-shaped JV-curve.

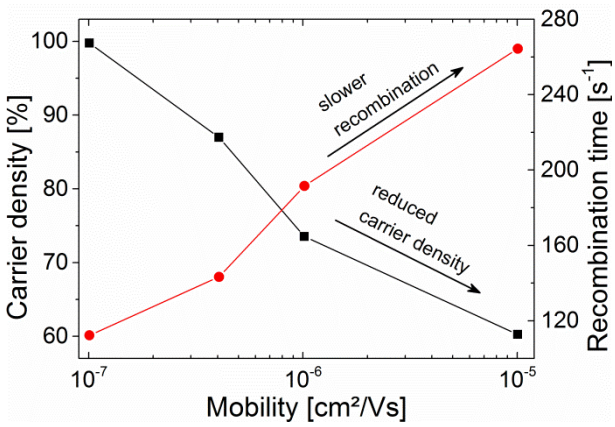

Figure 6 - Charge density and carrier life time within the device as a function of HSL mobility at the maximum power point. It can be seen that as HSL mobility increases, overall carrier density in the device decreases and carrier life time is extended, resulting in a more efficient solar cell.

5. Conclusion

We fabricated a series of organic solar cells with different hole selective layers comprising of evaporated pure TPD, TPD:HATCN mixtures and pure HATCN. By changing the composition of the HSL, we were able to tune its mobility between 10^{-7} and 10^{-5} cm^2/Vs. We showed that a device with a pure HATCN layer produced devices without s-shaped JV-curves. Using a HATCN doped TPD film as HSL we reduced the mobility of the HSL by reducing the HATCN ratio, and generated devices with s-shaped JV-curves. The change of mobility due to the crystallization of the pure TPD film could be used to separate the influence of mobility and energetic barrier on the s-shape. Numerical simulations confirmed that a low hole mobility in the HSL could produce an s-shaped JV-curve. Consequently, particular attention should be paid to the mobility of the hole selective layer to obtain long-term device stability.

Acknowledgements

We thank the German Research Foundation (DFG) within the priority program SPP 1355 ("Elementary Processes of Organic Photovoltaics") and the Bavarian State Ministry of Science, Research and the Arts within the collaborative research network "Solar Technologies go Hybrid". U.H. acknowledges the Bavarian Research Foundation for financial support and L.S. thanks Hans-Joachim Egelhaaf for fruitful discussions.

Appendix A. Supplementary material

Supplementary material associated with this article can be found in the online version at URL.

References

[1] C.J. Brabec, S.E. Shaheen, C. Winder, N.S. Sariciftci, P. Denk, Effect of LiF/metal electrodes on the performance of plastic solar cells, Appl. Phys. Lett. 80 (2002) 1288. doi:10.1063/1.1446988.

[2] W. Ma, C. Yang, X. Gong, K. Lee, A.J. Heeger, Thermally Stable, Efficient Polymer Solar Cells with Nanoscale Control of the Interpenetrating Network Morphology, Adv. Funct. Mater. 15 (2005) 1617–1622. doi:10.1002/adfm.200500211.

[3] G. Zhao, Y. He, Y. Li, 6.5% Efficiency of Polymer Solar Cells Based on poly(3-hexylthiophene) and Indene-C60 Bisadduct by Device Optimization, Adv. Mater. 22 (2010) 4355–4358. doi:10.1002/adma.201001339.

[4] J. Guo, H. Ohkita, H. Benten, S. Ito, Charge Generation and Recombination Dynamics in Poly(3-hexylthiophene)/Fullerene Blend Films with Different Regioregularities and Morphologies, J. Am. Chem. Soc. 132 (2010) 6154–6164. doi:10.1021/ja100302p.

[5] M.A. Green, K. Emery, Y. Hishikawa, W. Warta, E.D. Dunlop, Solar cell efficiency tables (version 39): Solar cell efficiency tables (version 39), Prog. Photovolt. Res. Appl. 20 (2012) 12–20. doi:10.1002/pip.2163.

[6] http://www. heliatek. com/newscenter/latest_news/neuer-weltrekord-fur-organische-solarzellen-heliatek-behauptet-sich-mi.-12-zelleffizienz-als-technologiefuhrer/?lang=en Heliatek GmbH, Heliatek consolidates its technology leadership by establishing a new world record for organic solar technology with a cell efficiency of 12%, (2013). http://www.heliatek.com/newscenter/latest_news/neuer-weltrekord-fur-organische-solarzellen-heliatek-behauptet-sich-mit-12-zelleffizienz-als-technologiefuhrer/?lang=en (accessed August 19, 2013).

[7] C.J.M. Emmott, A. Urbina, J. Nelson, Environmental and economic assessment of ITO-free electrodes for organic solar cells, Sol. Energy Mater. Sol. Cells. 97 (2012) 14–21. doi:10.1016/j.solmat.2011.09.024.

[8] F.C. Krebs, S.A. Gevorgyan, J. Alstrup, A roll-to-roll process to flexible polymer solar cells: model studies, manufacture and operational stability studies, J. Mater. Chem. 19 (2009) 5442. doi:10.1039/b823001c.

[9] M.M. Voigt, R.C.I. Mackenzie, C.P. Yau, P. Atienzar, J. Dane, P.E. Keivanidis, et al., Gravure printing for three subsequent solar cell layers of inverted structures on flexible substrates, Sol. Energy Mater. Sol. Cells. 95 (2011) 731–734. doi:10.1016/j.solmat.2010.10.013.

[10] A. Wagenpfahl, D. Rauh, M. Binder, C. Deibel, V. Dyakonov, S-shaped current-voltage characteristics of organic solar devices, Phys. Rev. B. 82 (2010) 115306. doi:10.1103/PhysRevB.82.115306.

[11] F.A. de Castro, J. Heier, F. Nuesch, R. Hany, Origin of the Kink in Current-Density Versus Voltage Curves and Efficiency Enhancement of Polymer-C60 Heterojunction Solar Cells, IEEE J. Sel. Top. Quantum Electron. 16 (2010) 1690–1699.

[12] J. Wagner, M. Gruber, A. Wilke, Y. Tanaka, K. Topczak, A. Steindamm, et al., Identification of different origins for s-shaped current voltage characteristics in planar heterojunction organic solar cells, J. Appl. Phys. 111 (2012) 054509. doi:10.1063/1.3692050.

[13] W. Tress, A. Petrich, M. Hummert, M. Hein, K. Leo, M. Riede, Imbalanced mobilities causing S-shaped IV curves in planar heterojunction organic solar cells, Appl. Phys. Lett. 98 (2011) 063301. doi:10.1063/1.3553764.

[14] W. Tress, K. Leo, M. Riede, Influence of Hole-Transport Layers and Donor Materials on Open-Circuit Voltage and Shape of I-V Curves of Organic Solar Cells, Adv. Funct. Mater. 21 (2011) 2140–2149. doi:10.1002/adfm.201002669.

[15] L. Chkoda, C. Heske, M. Sokolowski, E. Umbach, F. Steuber, J. Staudigel, et al., Work function of ITO substrates and band-offsets at the TPD/ITO interface determined by photoelectron spectroscopy, Synth. Met. 111-112 (2000) 315–319.
[16] J. Yang, K.C. Gordon, Organic light emitting devices based on exciplex interaction from blends of charge transport molecules, Chem. Phys. Lett. 375 (2003) 649–654.
[17] C. Falkenberg, S. Olthof, R. Rieger, M. Baumgarten, K. Muellen, K. Leo, et al., The role of energy level matching in organic solar cells—Hexaazatriphenylene hexacarbonitrile as transparent electron transport material, Sol. Energy Mater. Sol. Cells. 95 (2011) 927–932.
[18] M.O. Reese, M.S. White, G. Rumbles, D.S. Ginley, S.E. Shaheen, Optimal negative electrodes for poly (3-hexylthiophene):[6, 6]-phenyl C61-butyric acid methyl ester bulk heterojunction photovoltaic devices, Appl. Phys. Lett. 92 (2008) 053307–053307.
[19] I. Park, Y. Lim, S. Noh, D. Lee, M. Meister, J.J. Amsden, et al., Enhanced photovoltaic performance of ZnO nanoparticle/poly(phenylene vinylene) hybrid photovoltaic cells by semiconducting surfactant, Org. Electron. 12 (2011) 424–428. doi:10.1016/j.orgel.2010.12.002.
[20] K. Kawano, R. Pacios, D. Poplavskyy, J. Nelson, D.D.C. Bradley, J.R. Durrant, Degradation of organic solar cells due to air exposure, Sol. Energy Mater. Sol. Cells. 90 (2006) 3520–3530. doi:10.1016/j.solmat.2006.06.041.
[21] A. Seemann, T. Sauermann, C. Lungenschmied, O. Armbruster, S. Bauer, H.-J. Egelhaaf, et al., Reversible and irreversible degradation of organic solar cell performance by oxygen, Sol. Energy. 85 (2011) 1238–1249. doi:10.1016/j.solener.2010.09.007.
[22] S.K. Hau, H.-L. Yip, N.S. Baek, J. Zou, K. O'Malley, A.K.-Y. Jen, Air-stable inverted flexible polymer solar cells using zinc oxide nanoparticles as an electron selective layer, Appl. Phys. Lett. 92 (2008) 253301. doi:10.1063/1.2945281.
[23] J. Meyer, A. Kahn, Electronic structure of molybdenum-oxide films and associated charge injection mechanisms in organic devices, J. Photonics Energy. 1 (2011) 011109–011109.
[24] See supplementary material at [URL] for more information, Foot note 1, (n.d.).
[25] K. Naito, A. Miura, Molecular design for nonpolymeric organic dye glasses with thermal stability: relations between thermodynamic parameters and amorphous properties, J. Phys. Chem. 97 (1993) 6240–6248.
[26] T. Krieg, A. Petr, G. Barkleit, L. Dunsch, Improved thermal stability of nonpolymeric organic glasses by doping with fullerene C60, Appl. Phys. Lett. 74 (1999) 3639–3641.
[27] L.J.A. Koster, V.D. Mihailetchi, P.W.M. Blom, Bimolecular recombination in polymer/fullerene bulk heterojunction solar cells, Appl. Phys. Lett. 88 (2006) 052104. doi:10.1063/1.2170424.
[28] R. Hanfland, M.A. Fischer, W. Brütting, U. Würfel, R.C.I. MacKenzie, The physical meaning of charge extraction by linearly increasing voltage transients from organic solar cells, Appl. Phys. Lett. 103 (2013) 063904. doi:10.1063/1.4818267.
[29] F. Deschler, D. Riedel, B. Ecker, E. von Hauff, E. Da Como, R.C.I. MacKenzie, Increasing organic solar cell efficiency with polymer interlayers, Phys. Chem. Chem. Phys. 15 (2013) 764. doi:10.1039/c2cp43876c.
[30] R.C.I. MacKenzie, C.G. Shuttle, M.L. Chabinyc, J. Nelson, Extracting Microscopic Device Parameters from Transient Photocurrent Measurements of P3HT:PCBM Solar Cells, Adv. Energy Mater. 2 (2012) 662–669. doi:10.1002/aenm.201100709.
[31] See supplementary material at [URL] for the full set of parameters used in the simulation, Foot note 3, (n.d.).
[32] Estimated, see supplementary material for more information, Foot note 2, (n.d.).